OXFORD UNIVERSITY PRESS | Cerebral Cortex

Contour integration over time: Psychophysical and fMRI evidence

Journal:	*Cerebral Cortex*
Manuscript ID	CerCor-2015-00474.R3
Manuscript Type:	Original Articles
Date Submitted by the Author:	n/a
Complete List of Authors:	Kuai, Shu-Guang; East China Normal University, Psychology Li, Wu; Beijing Normal University, Brain and Cognition Yu, Cong; Peking University, Department of Psychology Kourtzi, Zoe; University of Cambridge, Psychology
Keywords:	contour integration, Gestalt, good continuity, psychophysics, fMRI

Contour integration over time: Psychophysical and fMRI evidence

Shu-Guang Kuai[1], Wu Li[2], Cong Yu[3], and Zoe Kourtzi[4]

[1] MOE and Shanghai Key Laboratories of Brain Functional Genomics and School of Psychology and Cognitive Science, East China Normal University, Shanghai, China;

[2] State Key Laboratory of Cognitive Neuroscience and Learning and IDG/McGovern Institute for Brain Research, Beijing Normal University, Beijing, China;

[3] Department of Psychology, IDG/McGovern Institute for Brain Research, and Peking-Tsinghua Center for Life Sciences, Peking University, Beijing, China;

[4] Department of Psychology, University of Cambridge, Cambridge, UK.

Corresponding authors:

Cong Yu, Department of Psychology, Peking University, 100181, Beijing, China; 86-10-6275-7056; yucong@pku.edu.cn.

Zoe Kourtzi, Department of Psychology, University of Cambridge, CB2 3AR, UK; zk240@cam.ac.uk

Running title:

Contour integration over time

Abstract

The brain integrates discrete but collinear stimuli to perceive global contours. Previous contour integration (CI) studies mainly focus on integration over space, and CI is attributed to either V1 long-range connections, or contour processing in high visual areas that top-down modulate V1 responses. Here we show that CI also occurs over time in a design that minimizes the roles of V1 long-range interactions. We use tilted contours embedded in random orientation noise and move horizontally behind a fixed vertical slit. Individual contour elements traveling up/down within the slit would be encoded over time by parallel, rather than aligned, V1 neurons. However, we find robust contour detection even when the slit permits only one viewable contour element. Similar to CI over space, CI over time also obeys the rule of collinearity. fMRI evidence shows that while CI over space engages visual areas as early as V1, CI over time mainly engages higher dorsal and ventral visual areas involved in shape processing, as well as posterior parietal regions involved in visual memory that can represent the orientation of temporally integrated contours. These results suggest at least partially dissociable mechanisms for implementing the Gestalt rule of continuity in CI over space and time.

Key words: contour integration, Gestalt principles, good continuity, psychophysics, fMRI

Integrating local image fragments into global shapes is critical for object recognition in complex environments. This contour integration (CI) process has been extensively investigated in psychophysical, neurophysiological, neuroimaging, and computational modeling studies (e.g., Field DJ et al. 1993; Li Z 1998; Kourtzi Z et al. 2003; Li W et al. 2006). However, the neural mechanisms under CI remain controversial. One distinct characteristic is that it follows the Gestalt rule of good continuation. That is, adjacent contour segments that are similarly oriented and aligned are more likely to be integrated. Because long-range horizontal connections in V1 are known to connect neurons with similar orientation preferences (Gilbert CD and TN Wiesel 1989), many contour integration theories assume that such connections would mediate contour integration through contextual modulation (e.g., Field DJ *et al.* 1993; Li Z 1998; Kapadia MK et al. 2000).

However, neuroimaging evidence indicates that CI involves multiple areas from V1 to LOC (Altmann CF et al. 2003; Kourtzi Z *et al.* 2003). There are reports that high-level visual regions such as LOC are activated earlier than V1 by contour stimuli (Mijovic B et al. 2013; Shpaner M et al. 2013). These results are consistent with monkey data that contour-related responses in V1 are delayed with respect to initial neural responses to visual stimuli (Li W *et al.* 2006; Gilad A et al. 2013; Chen M et al. 2014), and that V1responses to contour stimuli are strongly modulated by top-down feedback (Li W *et al.* 2006, 2008; McManus JN et al. 2011; Chen M *et al.* 2014). However, it is unclear whether V1 horizontal connections are an indispensable machinery for contour integration under all viewing conditions.

In this study we examine whether CI could still take place in a viewing condition where V1 horizontal connections are likely rendered ineffective. We ask the observers to detect a collinear contour embedded in random orientation noise, which is similar to stimuli used in many CI studies (e.g., Field et al., 1993), while the whole stimulus image is moving behind a fixed vertical slit (Fig. 1a). The contour is tilted while the whole stimulus image moves horizontally. Therefore, the viewable elements of the contour move either up or down within the vertical slit, one at a time. These contour elements would be encoded over time by V1 neurons that are not arranged along the contour path, but are parallel to each other. If the contour is still detectable when the slit is narrow enough to allow only up to one contour element to be viewed at any moment, we would argue that V1 horizontal connections may not play a significant role in this particular temporal integration process. Rather, we reason that higher-level mechanisms responsible for visual working memory and shape perception may play more prominent roles.

Materials and Methods

Observers

Twenty-two observers (12 males and 10 females, mean age = 24 years) with normal or corrected-to-normal vision participated in psychophysical and fMRI experiments. Some observers participated in more than one psychophysical and/or fMRI experiments (see Results). All except KG, the first author, were new to psychophysical and fMRI experiments and were unaware of the purposes of the study. Informed written consent was obtained from each observer prior to data collection.

Stimuli

The stimuli comprised of 256 Gabors (Gaussian windowed sinusoidal gratings), each occupying one of 16 × 16 invisible square grids (0.825° × 0.825° each). Some Gabors formed collinear contour paths, and the remaining ones were randomly oriented. The Gabors had a spatial frequency at 3 cpd, a standard deviation at 0.15°, and a contrast at 70%. The phases of the Gabors varied randomly from 0º to 315º in 45º steps. When slit-viewed the stimulus image moved behind a vertical slit at a speed of 6.4º/s in psychophysical experiments or 6.8º/s in fMRI experiments.

In psychophysical experiments, a straight contour path formed by nine collinear Gabor elements was embedded in a field of randomly oriented Gabors (Fig 1a). The center of the path was randomly positioned within a range of ±2.5º from the stimulus center. To control the density cues, the center-to-center horizontal distance of adjacent contour elements varied from 0.9 to 1.1 times the average inter-element distance (AIED) that was equal to the grid width. The global orientation of the contour path was randomized either between 15º-60º or between 120º-165º. A random stimulus image (without any contour path) was also generated within the same trial in a different stimulus interval by randomly shuffling the positions of all Gabors in the contour stimulus image.

In fMRI experiments, to maintain a sufficiently strong signal-to-noise ratio of BOLD responses, each contour stimulus image consisted of five nearly parallel contour, each containing 4-10 Gabor elements. The five contours of different lengths were randomly placed, and the distance between two neighboring contours was randomized from 1.5º to 2.25º. The global orientation of each contour was randomized from 30-45º or from 135-150º.

All stimuli were generated with Matlab-based Psychtoolbox3 (Pelli DG 1997). In psychophysical experiments the stimulus images were presented on a 21-inch CRT monitor (1280 × 1024 pixels, 0.3 mm × 0.3 mm pixel size, 85 Hz frame rate, and 47 cd/m^2 mean luminance). The luminance of the monitor was linearized by an 8-bit look-up table. Viewing was binocular at a distance of 46 cm. A chin-and-head rest was used to stabilize the head of the observer. Experiments were run in a dimly lit room. In fMRI experiments, the stimuli were presented through a projector onto a mirror in front of the observer (1280 × 1024 pixels, 0.44 mm × 0.44 mm pixel size, 60 Hz frame rate). The luminance of the projector was linearized by an 8-bit look-up table. Viewing was binocular at a distance of 67 cm.

Psychophysical procedure

Contour detection performance was measured with a two-interval forced-choice (2IFC) method of constant stimuli. In each trial, the stimulus image moved behind a vertical slit of various widths from left to right or reversely for 2 s. Two stimulus intervals, one containing the contour image and the other containing the random stimulus image, were separated by a 500-ms inter-stimulus interval. Observers were instructed to report which interval contained a contour. Each slit width was repeated in 60 trials.

fMRI experimental procedure

Each observer was scanned for 7-8 runs using a block design. Each run consisted of 16 stimulus blocks that were interleaved with 3 fixation blocks (10 s each) at the beginning, in the middle, and at the end of the run, respectively. Each stimulus block consisted of 8 trials and lasted for 20 s. Each trial consisted of a 2-s stimulus image and

a 0.5-s blank with slit viewing, or four 0.5-s regenerated similar stimulus images (to minimize adaptation) and a 0.5-s blank with full-field viewing. The color of the fixation dot changed in 25% of the trials randomly. Color changes never occurred in two consecutive trials. Observers were asked to report the stimulus type (e.g., contour or random stimulus) when color changed. Since the participants could not predict the trials to which they needed to be respond, they had to keep their attention to the stimulus images throughout the experimental runs.

fMRI Data Acquisition

fMRI data were acquired in a 3T Achieva Philips scanner at the University of Birmingham Imaging Centre using an eight-channel head coil. Anatomical images were obtained using a three-dimensional T1-weighted sequence (voxel size = 1 × 1 × 1 mm, slices = 175) for localization and visualization of the functional data. Functional images were acquired by a high-resolution gradient echo-pulse sequence covering the occipital and posterior temporal cortex (28 slices; TR: repetition time = 2000ms; TE: time to echo = 34 ms; resolution = 1.5 × 1.5 × 2 mm).

fMRI data analysis

Anatomical data were transformed into Talairach space and then inflated using BrainVoyager QX (Brain Innovations, Maastricht, Netherlands). Pre-processing of functional data included slice scan time correction, three-dimensional motion correction, linear trend removal, and temporal high-pass filtering (3 cycles per run), but not spatial smoothing. Trials with head motion larger than 1 mm of translation or 1 degree of rotation were excluded from analysis (<5% of total trials). The functional images were aligned to anatomical data and the complete data were transformed into

Talairach space. For each observer, the functional imaging data between the two sessions were co-aligned, registering all volumes for each observer to the first functional volume of the first run and session. This procedure ensured a cautious registration across sessions.

Regions of interest

For each individual observer, we identified retinotopic motion-related (V3B/KO) and shape-related (LO) areas using standard procedures. Specifically, visual areas (V1, V2, V3, V3a, hV4, V7) were defined by standard retinotopic mapping procedures using rotating wedge stimuli (Engel SA et al. 1994; Sereno MI et al. 1995; DeYoe EA et al. 1996). hV4 was identified as the region comprising the ventral but not the dorsal subregion of V4 (Wandell BA et al. 2007). V3B/KO was defined as the set of contiguous voxels anterior to V3A and inferior to V7 showing significantly higher response to kinetic boundaries than transparent motion (Dupont P et al. 1997; Zeki S et al. 2003). One observer in the full-field viewing condition did not complete the localizer scan of V3B/KO. For this observer, we defined the V3B/KO based on known Talairach coordinates for this region (left hemisphere: -29.5, -83.9, 1.8; right hemisphere: 31.5, -81.4, 3.6). Area MT was defined as the set of voxels in the lateral temporal cortex demonstrating significantly higher activation to an array of moving dots than to a static array dots (Zeki S et al. 1991). LO was defined as a set of contiguous voxels in the posterior ventral occipitotemporal cortex showing significantly stronger activation for intact than for scrambled images (Malach R et al. 1995; Kourtzi Z and N Kanwisher 2001). Note that the anterior LOC subregions and ventral regions around the fusiform and the parahippocampal gyrus were not included since they were covered by high-resolution slices scanned in this study. Finally,

intraparietal areas (VIPS, left hemisphere: -24.2, -73.2, 25, right hemisphere: 27.4, -72, 25.8 and POIPS, left hemisphere: -20.3, -66.1, 42.6, right hemisphere: -20.8, -65.2, 42.7) were defined on the basis of known Talairach coordinates for these regions (Orban GA et al. 1999) since we did not have a functional localizer for these areas. Data from different hemispheres were merged for further analysis. The final ROIs spanned both hemispheres, as both hemispheres showed the same pattern of results.

Multi-voxel pattern analysis

To identify brain patterns that discriminate between stimuli (e.g. contour vs. random stimuli, or left- vs. right-tilted contour paths), we performed multi-voxel pattern classification analysis (Haynes JD and G Rees 2005; Kamitani Y and F Tong 2005). Voxels that showed stronger responses for all stimulus conditions compared to fixation were selected and ranked in descending-order based on their t-values. The first 500 voxels for each ROI per observer were then selected for analysis, as prediction accuracy had saturated at this pattern size across areas. The time course of each voxel was extracted and normalized (z-score) in each run to minimize baseline differences across runs. The fMRI data were shifted by 4s due to the hemodynamic response delay and were then averaged within each experimental block.

We trained binary linear support vector machine (SVM) classifiers to discriminate fMRI responses evoked by contour vs. random stimuli or by different contour orientations using a leave-one-run-out cross-validation procedure. There were 112-128 training patterns and 16 test patterns in the slit viewing fMRI experiment, and 64 training patterns and 8 test patterns in the full-field viewing fMRI experiment. It is important to note that the classification comparisons were independent of the voxel

selection procedure (stimulus vs. fixation). Specifically, we ranked voxels by their activations to all stimulus conditions in contrast to the fixation condition and selected the top 500 voxels in each ROI. That is, voxel selection was independent of pattern classification contrasts (e.g., contour vs. random), avoiding circularity in the MVPA analyses procedures. Further, we subtracted the univariate signal for each condition to prevent MVPA classification relying simply on differences in fMRI responses between stimulus conditions. That is, for each run the mean fMRI signal across volumes per condition was subtracted from the fMRI signal per volume. For each observer, we calculated the mean accuracy of the classifier's predictions over cross-validations. To calculate the classifier's baseline performance, stimulus labels were randomly assigned to experimental blocks and the same MVPA analysis as described above was conducted for 1000 times. In addition, the distribution of classification accuracies was estimated from actual data by 1000 times of bootstrap resampling. The probability of overlap between distributions of classifier predictions using ordered vs. shuffled stimulus labels was estimated to assess significance.

Results

Psychophysical experiments

We found that when the contour stimulus moved behind a narrow fixed (non-moving) slit that allowed as few as one contour element to be viewed at any given moment (Fig. 1a), the global contour was still detectable. Six observers' data showed that contour detection was near chance when measured at a slit width of 0.2 times the average inter-element distance (AIED, Fig. 1b). However, the performance was

improved to ~70% correct when the slit width was increased to 0.4 AIED, where only one contour element or part of it was visible at any given moment. The slope of a line connecting the data points at 0.2 and 0.4 AIED was 0.86. A further increase of the slit width to 0.8 AIED, where parts of two neighboring contour elements were sometimes visible at the same time, elevated contour detection rate to ~80%, but at a much slower speed (slope = 0.19). There was additional slight improvement of performance by approximately 6.4% as the slit width increased from 1 to 2 AIED when two neighboring contour elements were sometimes fully visible at the same time (slope = 0.06). Further increasing the slit width, which allowed spatial interaction of neighboring contour elements, had a smaller incremental impact on contour detection. These results show that global contour detection under the slit-viewing condition is possible with temporal integration of neighboring contour elements. As we pointed out earlier, such contour processing with our particular stimulus configurations may not be mediated by V1 horizontal connections.

CI over space is known to obey the Gestalt rule of good continuity (Field DJ *et al.* 1993). To examine whether collinearity is also crucial for CI over time, four observers from the previous experiment (Fig. 1b) perform the contour detection task again. However, the orientations of individual contour elements were now jittered within a range of 0º, ±10º, ±20º, ±30º, or ±45º from the contour path while the slit was 1 AIED wide. Contour detection deteriorated with increasing orientation jitter and reached chance level at ±45° orientation jitter (Fig. 1c). These results indicate that collinearity is as important in CI over time as over space.

As a control, we examined whether contour detection could be alternatively due to the perception of similarly oriented contour elements along the slit over time through a simple probability summation mechanism across time. Contour detection

performance was compared with iso-oriented contour elements all deviating from the contour path by 0° to 90° at steps of 15°. Such orientation deviations reduced collinearity while keeping the local orientation similarity unchanged. The same four observers from Fig. 1c performed this experiment. Their detection performance decreased as the orientation deviation increased, reaching the chance level when the orientation deviation was larger than 30° (Fig. 1d). The performance slightly recovered when the contour elements were all orthogonal to the path (90° deviation). Therefore, the potential detection of similarly oriented contour elements along the vertical slit could not account for contour detection under the slit-viewing condition.

For the collinear contour stimuli shown in Figure 1a, the observers might have responded on the basis of a barber-pole-illusion kind of percept: The up or down movements of the contour elements along the vertical slit. This possibility has not been completely ruled out by Fig. 1d because in the latter experiment the orientation of contour elements deviated from the contour path. To further examine this possibility, we separately jittered the positions of individual contour elements along the direction perpendicular to the contour path. This lateral position jitter destroyed the collinearity without changing the orientations of the contour elements. As a result, the up or down motions of individual contour elements were largely unchanged when viewed through the narrow slit, and so was the potential barber-pole illusion. Data from four observers showed that the contour detection performance started to decrease after the average position jitter was over ±0.5 AIED, and rapidly approached the chance level when the

jitter was larger than ±1.5 AIED (Fig. 1e). These results suggest that contour detection under slit-viewing is unlikely a result of the barber-pole illusion.

fMRI experiments

The above psychophysical data suggest that CI over time may not necessarily involve V1 horizontal connections. We conducted the following fMRI experiments to examine the cortical mechanism underlying this new CI format.

In the first fMRI experiment, nine observers were presented with four types of stimuli with slit-viewing in a blocked design: right-tilted contour stimuli (collinear contours oriented at 30°-45°, Fig. 2b) and their counterpart random images (all the positions of individual Gabors were randomly reshuffled), and left-tilted contour stimuli (collinear contours oriented at 150°-165°) and their counterpart random images. The ROIs shown in Fig. 2a include early, ventral and dorsal visual areas and IPS. These areas are highly relevant to visual information processing and were covered by our high-resolution fMRI sequence (1.5mm × 1.5mm × 2mm). However, a comparison of fMRI responses (i.e. percent signal change from the fixation baseline) between contour vs. random stimuli showed no significant differences in these ROIs ($F_{1,8} < 1$, $p = 0.60$, $\eta^2 = 0.036$). We thus used multi-voxel pattern analysis (MVPA), a more sensitive measure in discriminating activation patterns distributed across voxels.

We tested the accuracy of a linear support vector machine (SVM) in classifying fMRI signals associated with contour vs. random stimuli in each ROI. A repeated-measures ANOVA showed a significant effect of ROI ($F_{3.7, 30} = 7.18$, $p < 0.001$ with Greenhouse-Geisser correction, $\eta^2 = 0.473$). In particular, accuracies in higher dorsal visual areas (e.g. V3B/KO, $p = 0.003$), IPS (VIPS, $p = 0.016$; POIPS, $p < 0.001$), and LO ($p = 0.001$) were significantly higher than baseline as calculated by bootstrapping

(Fig. 2c; see Methods for baseline calculation). In contrast, no significant differences were observed in the early visual areas (V1, $p = 0.33$; V2, $p = 0.17$) and ventral visual areas (V3v, $p = 0.71$; hV4, $p = 0.34$).

We reasoned that contours could be perceived only after a number of local elements have been integrated over time. As a result, brain areas involved in visual memory should contain information that supports the discrimination of contours of different global orientations. To test this hypothesis, we examined fMRI selectivity for contour orientation by training a SVM classifier to discriminate activations for the right- vs. left-tilted contours (Fig. 2e). Only in POIPS was the classification accuracy significantly higher ($p = 0.001$) than baseline (Fig.2f), suggesting that POIPS, which is involved in visual memory (Linden DEJ et al. 2003; Todd JJ and R Marois 2004; Marois R and J Ivanoff 2005), may play a critical role in storing and integrating contour elements for CI over time (also see Discussion).

Next we measured fMRI responses to full-field stationary stimuli (the same right- and left-tilted contour stimuli and their counterpart random images used in the previous experiment, which were no longer viewed through a slit) in seven observers to compare brain areas involved in CI over space vs. over time. Detection performance (hit rate) was over 90% for contours and random stimuli (Fig. 3a). Again MVPA was used to discriminate between activations for contours vs. random stimuli. In contrast to CI over time, the classification accuracies were now significantly higher than baseline ($p < 0.001$) across all ROIs, including visual areas as early as V1 (Fig. 3b), consistent with previous fMRI results (Kourtzi Z *et al.* 2003). In addition, MVPA was also used to discriminate activations for different contour orientations (Fig. 3c-d), which also showed different classification accuracies across ROIs ($F_{3.4, 20.4} = 13.03$, $p < 0.001$, $\eta^2 = 0.685$). The accuracies were significantly higher than the baseline in early visual

areas V1 ($p = 0.001$) and V2 ($p < 0.001$), early ventral and dorsal visual areas V3d ($p < 0.001$) and V3a ($p < 0.001$), but not in higher dorsal visual areas V3b/KO ($p = 0.12$) and V7 ($p = 0.14$), posterior parietal regions VIPS ($p = 0.21$) and POIPS ($p = 0.36$), and LO ($p = 0.27$). The lack of significant accuracies in LO may be due to neural populations that are size and orientation invariant in this region (Grill-Spector K et al. 1999).

In Fig. 1a, when the stimulus contained a diagonal contour path, a single contour element moved upward or downward along the slit. Such vertical motion was not present when the stimulus contained no contour. Fig. 1d shows that when the contour elements were all equally rotated from the contour path by 30-75^{o}, contour detection deteriorated to chance levels. In these conditions a single contour element still moved upward or downward along the slit. Therefore the observers did not knowingly use the illusory motion as a cue for contour detection. However, even under these null-detection conditions, the motion cues could be extracted by neurons in V3A/B and other visual areas, and the classifier applied to fMRI data could discriminate between contour and random stimulus patterns based on signals related to these motion cues. Such a confound is more likely to be evident in our fMRI contour stimuli that contained five contours in a single stimulus, in contrast to one in psychophysical experiments. We ran a fMRI control experiment to test for this confound.

The stimuli patterns contained collinear contours, no contours, or contour stimuli with all elements oriented 45^{o} from the contour paths (“ladders”, Fig. 4a). Collinear contours and ladders resulted in similar vertical motion of local elements but only collinear contours produced coherent contour perception (Fig. 4b). We compared activation patterns in visual and posterior parietal areas when seven observers responded to collinear contours, ladders, and random stimuli. Performance detection was 83.4% for collinear contours and 45.7% for ladder contours, consistent with previous results that detection of ladder contours is impoverished (Schwarzkopf &

Kourtzi, 2008; Zhang & Kourtzi, 2010). MVPA was used to classify fMRI responses related to collinear vs. random stimuli and ladders vs. random stimuli (Fig. 4c). The classifier's performance for discriminating ladders vs. random contours was not significantly different from the baseline across ROIs. However, classification accuracy for collinear vs. random contours differed from the accuracy for ladders vs. random stimuli. There was a significant main effect of classifier (collinear vs. random and ladders vs. random, $F_{1,6} = 16.8$, $p = 0.006$, $\eta 2 = 0.737$) and a significant interaction between classifier and ROI ($F_{3.7,\ 22.1} = 3.9$, $p = 0.017$, $\eta 2 = 0.393$). Classification accuracy was significantly higher for collinear vs. random stimuli than for ladders vs. random stimuli in the dorsal visual areas ($F_{1,6} = 25.6$, $p = 0.002$, $\eta^2 = 0.81$), LO ($t(6) = 2.88$, $p = 0.028$, Cohen's $d = 1.09$), and IPS ($F_{1,6} = 21.51$, $p = 0.004$, $\eta^2 = 0.78$), but not in the early visual areas ($F_{1,6} = 1.35$, $p = 0.29$, $\eta^2 = 0.18$). Further, the classification accuracy showed a similar pattern between collinear vs. random stimuli and collinear vs. ladder stimuli. There were a non-significant main effect of classifier ($F_{1,6} = 1.5$, $p = 0.267$, $\eta^2 = 0.20$) and a non-significant interaction between classifier and ROI ($F_{3.5,\ 21.2} = 1.07$, $p = 0.39$, $\eta^2 = 0.15$), confirming that the activities in these areas reflect integration signals under slit-viewing. These results suggest that higher visual (ventral and dorsal) and posterior parietal regions contain information about the perceived contours under the slit-viewing condition, rather than the perceived vertical motion of similarly oriented contour elements.

We performed additional control analyses to examine whether the observed fMRI activation patterns could be due to differences in general arousal levels or eye movements. We did not observe any significant univariate BOLD signal differences between contour stimuli and random stimuli in the first fMRI experiment ($F_{1,8} < 1$, $p = 0.60$, $\eta^2 = 0.036$), suggesting that the fMRI results with the slit-viewing condition

could not be explained by higher general arousal levels for salient contours. Comparing slit-viewing (Fig. 2) and full-field viewing (Fig. 3) conditions did not reveal a significant main effect of viewing condition ($F_{1,14} < 1$, $p = 0.51$, $\eta^2 = 0.031$). Behavioral performance in contour detection did not differ between slit-viewing and full-field viewing either (90.9% ± 1.2% vs. 93.3% ± 4.2%, $t_{(14)} < 1$, $p = 0.55$, Cohen's $d = 0.29$). Thus the different activation patterns could not be explained by the differences in task difficulty that may alter observers' general arousal levels.

We recorded eye movements from four observers with an ASL 6000 Eye-tracker (Applied Science Laboratories, Bedford, MA, USA). Eye-tracking data were pre-processed with the Eyenal software from the same company and analyzed with custom Matlab code. For each stimulus condition, we calculated the horizontal and vertical eye positions and the amplitude and number of saccades. For each stimulus type, histograms of the horizontal and vertical eye positions were centered on the fixation at zero degree. Paired t-tests indicated no significant differences in horizontal eye position ($t_{(3)} < 1$, $p = 0.47$, Cohen's $d = 0.41$), vertical eye position($t_{(3)} < 1$, $p = 0.57$, Cohen's $d = 0.32$), number of saccades ($t_{(3)} < 1$, $p = 0.61$, Cohen's $d = 0.29$), horizontal saccade amplitude ($t_{(3)} = 1.3$, $p = 0.27$, Cohen's $d = 0.68$),and vertical saccade amplitude ($t_{(3)} < 1$, $p = 0.95$, Cohen's $d = 0.04$), regardless of whether the slit-viewed stimulus image contained contours or not. In addition, we did not find significant difference of eye positions in the first half and second half of a trial in the horizontal eye position ($F_{1,3} = 3.5$, $p = 0.16$, $\eta^2 = 0.54$), vertical eye position ($F_{1,3}<1$, $p = 0.41$, $\eta^2 = 0.23$), number of saccades ($F_{1,3} = 1.7$, $p = 0.29$, $\eta^2 = 0.36$), horizontal saccade amplitude ($F_{1,3} = 3.8$, $p = 0.15$, $\eta^2 = 0.56$), and vertical saccade amplitude ($F_{1,3} = 3.5$, $p = 0.16$, $\eta^2 = 0.54$), suggesting eye positions did not change systematically over time.

Discussion

Statistical analysis of natural scene images demonstrates that collinearity and co-circularity occur at a higher probability than other geometrical relationships (Sigman M and CD Gilber 2000; Geisler WS et al. 2001). These regularities well fit the Gestalt grouping rule of good continuity (Feldman J 2001; Geisler WS *et al.* 2001). Our slit-viewed contour stimuli by design minimize the roles of V1 long-range horizontal connections, so that the Gestalt rule of good continuation needs to be implemented by higher-level mechanisms. This is feasible since the visual system may acquire contour statistics from mechanisms that may not entirely rely on low-level V1 horizontal connections (Geisler WS *et al.* 2001). Indeed our fMRI evidence indicates the engagement of posterior parietal regions known to be involved in visual memory, and dorsal and ventral visual areas known to be involved in motion and shape processing, in CI over time.

Our fMRI results suggest that the posterior parietal cortex (POIPS) contains information related to the orientation of contours that are integrated over time (Fig. 2f). In contrast, ventral areas like LO that are representation invariant are ill-suited for the precise spatial and temporal encoding of contour elements that are integrated over time (Fig. 2f). POIPS is known to be involved not only in visual working memory (Todd JJ and R Marois 2004; Marois R and J Ivanoff 2005; Xu YD and MM Chun 2006), but also in attentional processing (Corbetta M et al. 1998). However, differential POIPS activation patterns for different contour orientations suggest that here POIPS is mainly responsible for CI over time in the visual memory, rather than for general attentional processing, consistent with other studies on slit-viewing (Mateeff S et al. 1993; Nishida S 2004; Silvanto J and Z Cattaneo 2010). The roles of the dorsal areas in global percepts defined by motion

signals have also been reported elsewhere (Caclin A et al. 2012; Zaretskaya N et al. 2013).

Our results also show that POIPS activation patterns cannot discriminate the orientations of full-field contours (Fig. 3d), consistent with Konen and Kastner (2008) in that regions of IPS are orientation-invariant for spatial stimuli. As the key difference between CI over space vs. time is the requirement of visual memory, the conflicting roles of POIPS in CI over space vs. time suggest that POIPS may be involved in short-term visual memory processes necessary for contour integration under slit-viewing. We speculate that POIPS memorizes orientations of contour elements passed through a slit and reconstruct the image of contour paths. The findings in agreement with previous studies showing that superior IPS maintains details of object features in visual memory (Bettencourt & Xu, 2016; Xu & Chun, 2006).

However, CI over time and space may share some component processes. Our fMRI evidence indicates that ventral areas like LO also participate in contour integration over time (Fig. 2d), and that both dorsal and ventral areas are involved in CI over space (Fig. 3b) as in other similar imaging studies (Altmann et al., 2003; Kourtzi et al., 2003; Murray, Foxe, Javitt, & Foxe, 2004; Murray et al., 2002; Shpaner et al., 2013). Moreover, 3D spatial contour interpolation, which involves integration of information from multiple depth cues, requires parietal areas as well (Kellman, Garrigan, & Shipley, 2005; Sakata, Taira, Kusunoki, Murata, & Tanaka, 1997). It is likely that, regardless of where and how the contour integration process is initially implemented in the brain, the higher-tier ventral areas responsible for global form processing, such as the LO, are necessary for global contour perception.

As a final note, in this study the exclusion of the roles of V1 horizontal connections in CI over time is based on the psychophysical stimulus design, not the null difference of V1 BOLD patterns between the contour and random stimuli (Fig. 2d). Because of the limited spatial resolution of fMRI, in principle a voxel is unable to

separate the activations by the contour and random stimuli (Guo et al., 2007), regardless of whether or not V1 neurons are able to detect the slit-viewed contours.

Acknowledgments

This research was supported by the European Community's Seventh Framework Programme (FP7/2007-2013) under grant agreement no 255577, the Biotechnology and Biological Sciences Research Council to ZK (D52199X, E027436), and National Natural Science Foundation of China Grants to CY (31230030) and to WL (91432102).

References

Altmann CF, Bulthoff HH, Kourtzi Z. 2003. Perceptual organization of local elements into global shapes in the human visual cortex. Curr Biol 13:342-349.

Caclin A, Paradis AL, Lamirel C, Thirion B, Artiges E, Poline JB, Lorenceau J. 2012. Perceptual alternations between unbound moving contours and bound shape motion engage a ventral/dorsal interplay. Journal of vision 12.

Chen M, Yan Y, Gong X, Gilbert CD, Liang H, Li W. 2014. Incremental integration of global contours through interplay between visual cortical areas. Neuron 82:682-694.

Corbetta M, Akbudak E, Conturo TE, Snyder AZ, Ollinger JM, Drury HA, Linenweber MR, Petersen SE, Raichle ME, Van Essen DC, Shulman GL. 1998. A common network of functional areas for attention and eye movements. Neuron 21:761-773.

DeYoe EA, Carman GJ, Bandettini P, Glickman S, Wieser J, Cox R, Miller D, Neitz J. 1996. Mapping striate and extrastriate visual areas in human cerebral cortex. Proc Natl Acad Sci U S A 93:2382-2386.

Dupont P, De Bruyn B, Vandenberghe R, Rosier AM, Michiels J, Marchal G, Mortelmans L, Orban GA. 1997. The kinetic occipital region in human visual cortex. Cerebral Cortex 7:283-292.

Engel SA, Rumelhart DE, Wandell BA, Lee AT, Glover GH, Chichilnisky EJ, Shadlen MN. 1994. fMRI of human visual cortex. Nature 369:525.

Feldman J. 2001. Bayesian contour integration. Percept Psychophys 63:1171-1182.

Field DJ, Hayes A, Hess RF. 1993. Contour integration by the human visual system: evidence for a local

"association field". Vision Res 33:173-193.

Geisler WS, Perry JS, Super BJ, Gallogly DP. 2001. Edge co-occurrence in natural images predicts contour grouping performance. Vision Res 41:711-724.

Gilad A, Meirovithz E, Slovin H. 2013. Population responses to contour integration: early encoding of discrete elements and late perceptual grouping. Neuron 78:389-402.

Gilbert CD, Wiesel TN. 1989. Columnar specificity of intrinsic horizontal and corticocortical connections in cat visual cortex. J Neurosci 9:2432-2442.

Grill-Spector K, Kushnir T, Edelman S, Avidan G, Itzchak Y, Malach R. 1999. Differential processing of objects under various viewing conditions in the human lateral occipital complex. Neuron 24:187-203.

Guo K, Robertson RG, Pulgarin M, Nevado A, Panzeri S, Thiele A, Young MP. 2007. Spatio-temporal prediction and inference by V1 neurons. Eur J Neurosci 26:1045-1054.

Haynes JD, Rees G. 2005. Predicting the orientation of invisible stimuli from activity in human primary visual cortex. Nat Neurosci 8:686-691.

Kamitani Y, Tong F. 2005. Decoding the visual and subjective contents of the human brain. Nat Neurosci 8:679-685.

Kapadia MK, Westheimer G, Gilbert CD. 2000. Spatial distribution of contextual interactions in primary visual cortex and in visual perception. Journal of Neurophysiology 84:2048-2062.

Konen CS, Kastner S. 2008. Two hierarchically organized neural systems for object information in human visual cortex. Nature neuroscience 11:224-231.

Kourtzi Z, Kanwisher N. 2001. Representation of perceived object shape by the human lateral occipital complex. Science 293:1506-1509.

Kourtzi Z, Tolias AS, Altmann CF, Augath M, Logothetis NK. 2003. Integration of local features into global shapes: monkey and human FMRI studies. Neuron 37:333-346.

Li W, Piech V, Gilbert CD. 2006. Contour saliency in primary visual cortex. Neuron 50:951-962.

Li W, Piech V, Gilbert CD. 2008. Learning to link visual contours. Neuron 57:442-451.

Li Z. 1998. A neural model of contour integration in the primary visual cortex. Neural Comput 10:903-940.

Linden DEJ, Bittner RA, Muckli L, Waltz JA, Kriegeskorte N, Goebel R, Singer W, Munk MHJ. 2003. Cortical capacity constraints for visual working memory: dissociation of fMRI load effects in a fronto-parietal network. Neuroimage 20:1518-1530.

Malach R, Reppas JB, Benson RR, Kwong KK, Jiang H, Kennedy WA, Ledden PJ, Brady TJ, Rosen BR, Tootell RB. 1995. Object-related activity revealed by functional magnetic resonance imaging in

human occipital cortex. Proceedings of the National Academy of Sciences of the United States of America 92:8135-8139.

Marois R, Ivanoff J. 2005. Capacity limits of information processing in the brain. Trends in Cognitive Sciences 9:296-305.

Marois R, Ivanoff J. 2005. Capacity limits of information processing in the brain. Trends Cogn Sci 9:296-305.

Mateeff S, Popov D, Hohnsbein J. 1993. Multi-aperture viewing: perception of figures through very small apertures. Vision Res 33:2563-2567.

McManus JN, Li W, Gilbert CD. 2011. Adaptive shape processing in primary visual cortex. Proceedings of the National Academy of Sciences of the United States of America 108:9739-9746.

Mijovic B, De Vos M, Vanderperren K, Machilsen B, Sunaert S, Van Huffel S, Wagemans J. 2013. The dynamics of contour integration: A simultaneous EEG-fMRI study. Neuroimage 88C:10-21.

Nishida S. 2004. Motion-based analysis of spatial patterns by the human visual system. Curr Biol 14:830-839.

Orban GA, Sunaert S, Todd JT, Van Hecke P, Marchal G. 1999. Human cortical regions involved in extracting depth from motion. Neuron 24:929-940.

Pelli DG. 1997. The VideoToolbox software for visual psychophysics: transforming numbers into movies. Spat Vis 10:437-442.

Sereno MI, Dale AM, Reppas JB, Kwong KK, Belliveau JW, Brady TJ, Rosen BR, Tootell RB. 1995. Borders of multiple visual areas in humans revealed by functional magnetic resonance imaging. Science 268:889-893.

Shpaner M, Molholm S, Forde E, Foxe JJ. 2013. Disambiguating the roles of area V1 and the lateral occipital complex (LOC) in contour integration. Neuroimage 69:146-156.

Sigman M, Gilber CD. 2000. Learning to find a shape. Nature Neurosci 3:264-269.

Silvanto J, Cattaneo Z. 2010. Transcranial magnetic stimulation reveals the content of visual short-term memory in the visual cortex. Neuroimage 50:1683-1689.

Todd JJ, Marois R. 2004. Capacity limit of visual short-term memory in human posterior parietal cortex. Nature 428:751-754.

Wandell BA, Dumoulin SO, Brewer AA. 2007. Visual field maps in human cortex. Neuron 56:366-383.

Xu YD, Chun MM. 2006. Dissociable neural mechanisms supporting visual short-term memory for objects. Nature 440:91-95.

Zaretskaya N, Anstis S, Bartels A. 2013. Parietal cortex mediates conscious perception of illusory

gestalt. The Journal of neuroscience : the official journal of the Society for Neuroscience 33:523-531.

Zeki S, Perry RJ, Bartels A. 2003. The processing of kinetic contours in the brain. Cerebral Cortex 13:189-202.

Zeki S, Watson JD, Lueck CJ, Friston KJ, Kennard C, Frackowiak RS. 1991. A direct demonstration of functional specialization in human visual cortex. The Journal of neuroscience : the official journal of the Society for Neuroscience 11:641-649.

Figure captions

Figure 1. Psychophysical results for CI over time under the slit-viewing condition. **a**. Stimuli: a collinear contour imbedded in random Gabors (left), random Gabors with no contour path (middle), and an example frame of the stimuli moving behind a non-moving slit (right). **b**. Contour detection as a function of the slit width. The smooth curve is the fit of a power function. AIED: average inter-element distance. **c**. Contour detection as a function of the +/- orientation jitter range of individual contour elements. **d**. Contour detection as a function of the uniform orientation deviation of all individual contour elements from the contour path. **e.** Contour detection as a function of the +/- position jitter perpendicular to the contour path. Error bars represent 1 standard error of the mean.

Figure 2. fMRI results for CI over time under slit-viewing conditions. **a**. ROIs in fMRI experiments. **b**. A stimulus image containing five right-tilted contour paths. **c**. The behavioral accuracies (hit rates) of judging whether the stimuli were contour stimuli or random Gabors. **d**. Mean MVPA accuracies for the classification of fMRI responses to contours vs. random Gabors. **e**. The behavioral accuracies (hit rates) of judging whether the contour stimuli were left-tilted or right-tilted. **f**. Mean MVPA accuracies for the classification of fMRI responses to left- vs. right-tilted contours. Dashed lines represent the mean upper limits of the 95% confidence interval calculated by shuffling the classification labels (upper confidence limits were very similar across ROIs).

Figure 3. fMRI results for CI over space. a. The behavioral accuracies (hit rates) of judging whether the stimuli were contour stimuli or random Gabors. b. Mean MVPA accuracy for the classification of fMRI responses to contours vs. random Gabors. c. The behavioral accuracies (hit rates) of judging whether the contour stimuli were left-tilted or right-tilted. d. Mean MVPA

accuracy for the classification of fMRI responses to left- vs. right-tilted contours. Dashed lines indicate the mean upper limits of the 95% confidence interval on the basis of bootstrap analysis.

Figure 4. fMRI results for CI over time under slit-viewing conditions with ladder contours. a. A stimulus images containing five ladder contours with all elements oriented 45° from the contour paths. The arrows indicate one contour path. b. The behavioral detection rates for collinear and ladder contours. c. MVPA accuracies for the classification of fMRI responses to collinear vs. random stimuli, collinear vs. ladder stimuli, and ladder vs. random stimuli. Dashed lines indicate the upper limits at a 95% confidence level from bootstrap analysis.

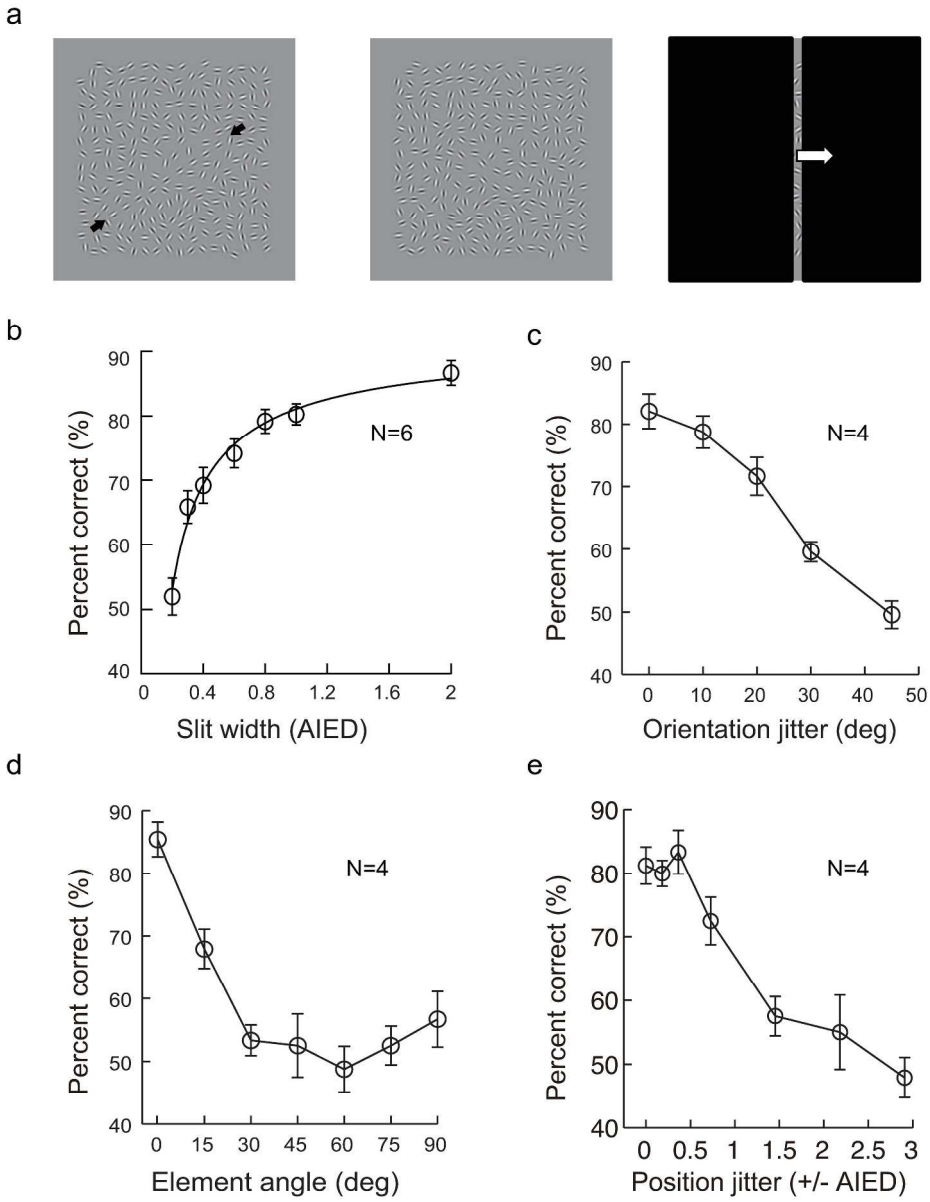

Figure 1. Psychophysical results for CI over time under the slit-viewing condition. a. Stimuli: a collinear contour imbedded in random Gabors (left), random Gabors with no contour path (middle), and an example frame of the stimuli moving behind a non-moving slit (right). b. Contour detection as a function of the slit width. The smooth curve is the fit of a power function. AIED: average inter-element distance. c. Contour detection as a function of the +/- orientation jitter range of individual contour elements. d. Contour detection as a function of the uniform orientation deviation of all individual contour elements from the contour path. e. Contour detection as a function of the +/- position jitter perpendicular to the contour path. Error bars represent 1 standard error of the mean.
257x335mm (300 x 300 DPI)

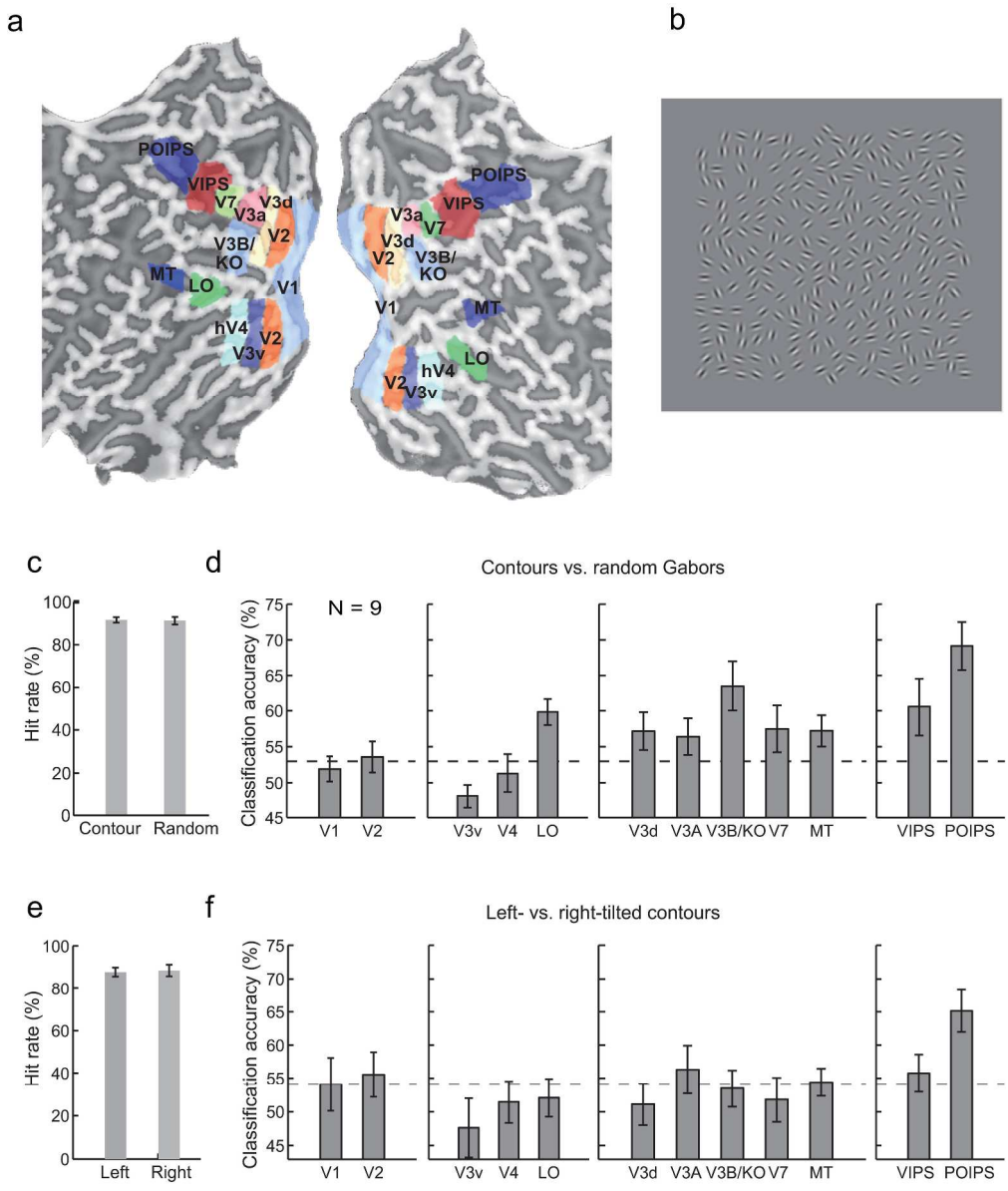

Figure 2. fMRI results for CI over time under slit-viewing conditions. a. ROIs in fMRI experiments. b. A stimulus image containing five right-tilted contour paths. c. The behavioral accuracies (hit rates) of judging whether the stimuli were contour stimuli or random Gabors. d. Mean MVPA accuracies for the classification of fMRI responses to contours vs. random Gabors. e. The behavioral accuracies (hit rates) of judging whether the contour stimuli were left-tilted or right-tilted. f. Mean MVPA accuracies for the classification of fMRI responses to left- vs. right-tilted contours. Dashed lines represent the mean upper limits of the 95% confidence interval calculated by shuffling the classification labels (upper confidence limits were very similar across ROIs).
247x292mm (300 x 300 DPI)

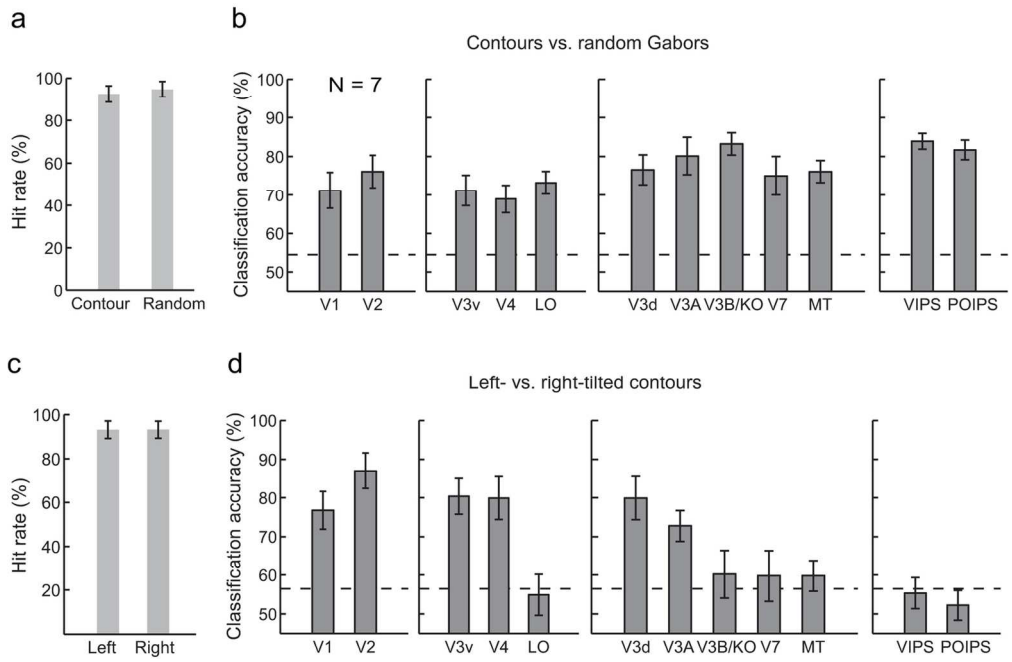

Figure 3. fMRI results for CI over space. a. The behavioral accuracies (hit rates) of judging whether the stimuli were contour stimuli or random Gabors. b. Mean MVPA accuracy for the classification of fMRI responses to contours vs. random Gabors. c. The behavioral accuracies (hit rates) of judging whether the contour stimuli were left-tilted or right-tilted. d. Mean MVPA accuracy for the classification of fMRI responses to left- vs. right-tilted contours. Dashed lines indicate the mean upper limits of the 95% confidence interval on the basis of bootstrap analysis.
137x90mm (300 x 300 DPI)

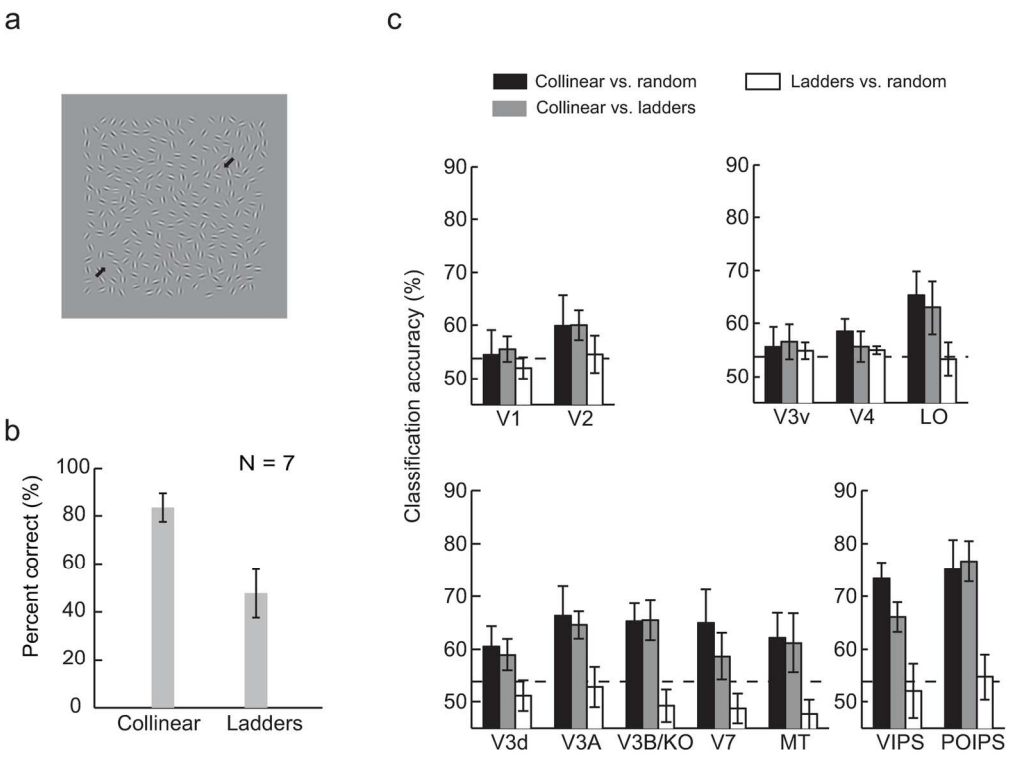

Figure 4. fMRI results for CI over time under slit-viewing conditions with ladder contours. a. A stimulus images containing five ladder contours with all elements oriented 45° from the contour paths. The arrows indicate one contour path. b. The behavioral detection rates for collinear and ladder contours. c. MVPA accuracies for the classification of fMRI responses to collinear vs. random stimuli, collinear vs. ladder stimuli, and ladder vs. random stimuli. Dashed lines indicate the upper limits at a 95% confidence level from bootstrap analysis.
150x113mm (300 x 300 DPI)